Marine and Petroleum Geology 28 (2011) 1768–1778

Contents lists available at ScienceDirect

Marine and Petroleum Geology

journal homepage: www.elsevier.com/locate/marpetgeo

Gas hydrate saturation in the Krishna–Godavari basin from P-wave velocity and electrical resistivity logs

Uma Shankar [a,1], Michael Riedel [b,*]

[a] National Geophysical Research Institute (Council of Scientific and Industrial Research, New Delhi) Hyderabad–500 606, India
[b] Natural Resources Canada, Pacific Geoscience Center, Geological Survey of Canada, 9860 W. Saanich Rd. Sidney, B.C. V8L 4B2, Canada

ARTICLE INFO

Article history:
Received 17 May 2010
Received in revised form
1 September 2010
Accepted 25 September 2010
Available online 2 October 2010

Keywords:
Gas hydrates
Krishna–Godavari basin
Electrical resistivity log
Archie analysis
P-Wave velocity logs
Effective medium modeling
Gas hydrate saturation
Volumetric estimation

ABSTRACT

During the Indian National Gas Hydrate Program (NGHP) Expedition 01, a series of well logs were acquired at several sites across the Krishna–Godavari (KG) Basin. Electrical resistivity logs were used for gas hydrate saturation estimates using Archie's method. The measured *in situ* pore-water salinity, seafloor temperature and geothermal gradients were used to determine the baseline pore-water resistivity. In the absence of core data, Arp's law was used to estimate *in situ* pore-water resistivity. Uncertainties in the Archie's approach are related to the calibration of Archie coefficient (a), cementation factor (m) and saturation exponent (n) values. We also have estimated gas hydrate saturation from sonic P-wave velocity logs considering the gas hydrate in-frame effective medium rock-physics model. Uncertainties in the effective medium modeling stem from the choice of mineral assemblage used in the model. In both methods we assume that gas hydrate forms in sediment pore space. Combined observations from these analyses show that gas hydrate saturations are relatively low (<5% of the pore space) at the sites of the KG Basin. However, several intervals of increased saturations were observed e.g. at Site NGHP-01-03 ($S_h = 15–20\%$, in two zones between 168 and 198 mbsf), Site NGHP-01-05 ($S_h = 35–38\%$ in two discrete zone between 70 and 90 mbsf), and Site NGHP-01-07 shows the gas hydrate saturation more than 25% in two zones between 75 and 155 mbsf. A total of 10 drill sites and associated log data, regional occurrences of bottom-simulating reflectors from 2D and 3D seismic data, and thermal modeling of the gas hydrate stability zone, were used to estimate the total amount of gas hydrate within the KG Basin. Average gas hydrate saturations for the entire gas hydrate stability zone (seafloor to base of gas hydrate stability), sediment porosities, and statistically derived extreme values for these parameters were defined from the logs. The total area considered based on the BSR seismic data covers ~720 km^2. Using the statistical ranges in all parameters involved in the calculation, the total amount of gas from gas hydrate in the KG Basin study area varies from a minimum of ~5.7 trillion-cubic feet (TCF) to ~32.1 TCF.

1. Introduction

Gas hydrate is a solid substance consisting of an ice lattice in which hydrocarbon molecules (mainly methane) are imbedded. Gas hydrate occurs widespread in the KG Basin, eastern continental margin of India (Collett et al., 2008a; Ramana et al., 2009). Marine gas hydrate generally occurs within the top few hundred meters of sediments in continental margins worldwide (e.g. Kvenvolden et al., 1993). The inclusion of gas hydrate in marine sediments usually changes the physical properties of the bulk sediment subsequently. Gas hydrate can take on many forms, including small nodules, lenses, veins, fracture-filling, and pore-filling. In the simplest model, rising methane combines with the sediment pore fluid to form gas hydrate, partially replacing the pore fluid (i.e. pore-filling), but little change to the sediment structure or volume. More complex models involve gas hydrate crystal growth by displacement of the ambient sediment, in form of veins, fracture-fill, small nodules, or lenses.

The presence of gas hydrate in-pore space of marine sediments can therefore significantly affect the bulk physical properties of the sediments. Gas hydrates exhibit relatively high compressional wave velocity compared to pore-filling fluids such as water; therefore, the velocity of gas hydrate bearing sediments are usually elevated (Stoll et al., 1971; Tucholkeb et al., 1977). Seismic velocities can be obtained from multichannel seismic data, Logging-while-drilling (LWD) down-hole sonic velocity, or vertical seismic profile (VSP)

* Corresponding author. Tel.: +1 250 363 6422; fax: +1 250 363 6565.
E-mail addresses: umashankar_ngri@yahoo.com (U. Shankar), mriedel@nrcan.gc.ca, mriedel@eps.mcgill.ca (M. Riedel).
[1] Tel.: +91 40 23434700x2510; fax: +91 40 23434651.

0264-8172/$ – see front matter
doi:10.1016/j.marpetgeo.2010.09.008

measurements (Westbrook et al., 1994; Yuan et al., 1996; Paull et al., 1996). Numerous studies have attempted to relate seismic velocity to gas hydrate saturation, using a variety of approaches. Most methods can be classified as empirical porosity–velocity relations applied to effective porosity reduction models (e.g., Hyndman et al., 1993; Yuan et al., 1996), time-averaging approaches (e.g., Pearson et al., 1983; Lee et al., 1993), and first-principles-based rock-physics modeling approaches (e.g., Dvorkin and Nur, 1993; Carcione and Tinivella, 2000; Helgerud et al., 1999).

From the various physical-property down-hole logs, resistivity appears to be the most strongly affected by the presence of gas hydrate in the marine sediment. Its inclusion in the pore space of marine sediments can significantly affect the bulk physical properties of the sediment. The measurement of such properties can therefore be used to estimate gas hydrate saturation (e.g. Collett and Ladd, 2000; Yuan et al., 1996). Natural gas hydrate formation reduces the effective porosity and electric conduction, so that gas hydrate bearing sediment has high electrical resistivity. Down-hole resistivity logs have been used extensively to characterize the *in situ* properties of gas hydrate bearing sediments and estimation of gas hydrate saturations (e.g., Collett and Ladd, 2000; Collett, 2002; Guerin et al., 1999; Helgerud et al., 1999; Hyndman et al., 2001; Lee and Collett, 2005; Lee and Waite, 2008).

In this study gas hydrate saturation estimates are described using Archie's (1942) law from the electrical resistivity log data and an effective medium modeling approach to predict the P-wave velocity for different amounts of gas hydrate saturation in the sediments.

In total 10 of the NGHP Expedition 01 gas hydrate sites from the KG Basin are used for the gas hydrate saturation estimates. Specifically we show results from Sites NGHP-01-03, NGHP-01-05 and NGHP-01-07, as representative examples. Site NGHP-01-03, in 1076 m of water, is in the southern portion of the KG Basin, Site NGHP-01-05, within 945 m of water, is located in the central part of basin. Site NGHP-01-07 is situated on the eastern most part of the basin at grater water depth around 1285 m (Fig. 1). We assume that the gas hydrate primarily replaces a portion of the sediment pore fluid, since no large pieces ("massive") of gas hydrate were recovered at these site and dispersed gas hydrate has been inferred (Collett et al., 2008a). The gas hydrate saturation versus resistivity may be quite different if there are massive gas hydrates that displace the sediment (e.g., Mathews, 1986). The problem for estimating gas hydrate saturation is how to separate the effects on the down-hole log resistivity data of the resistive hydrate and of the unusually low salinity *in situ* pore fluids. *In situ* pore fluid salinity measurements from direct down-hole sampling are not generally available. To obtain the effect of the gas hydrate on the measured resistivity, the *in situ* pore fluid salinity was inferred from the measurement of the interstitial properties of the pore fluid of the recovered core. Should core-derived values of pore-water salinity be unavailable, we invoke Arps' (1953) law to derive the *in situ* pore-water resistivity as function of down-hole temperature using regionally defined seafloor temperatures and thermal gradients, and seawater resistivity at the seafloor as input parameters (Collett et al., 2008a; Shankar et al., in press).

In the final part of this study we combine the observation of bottom-simulating reflectors (BSR) in 2D and 3D seismic data with the gas hydrate saturations defined from log-parameters to calculate a total volume of gas hydrate in the KG basin.

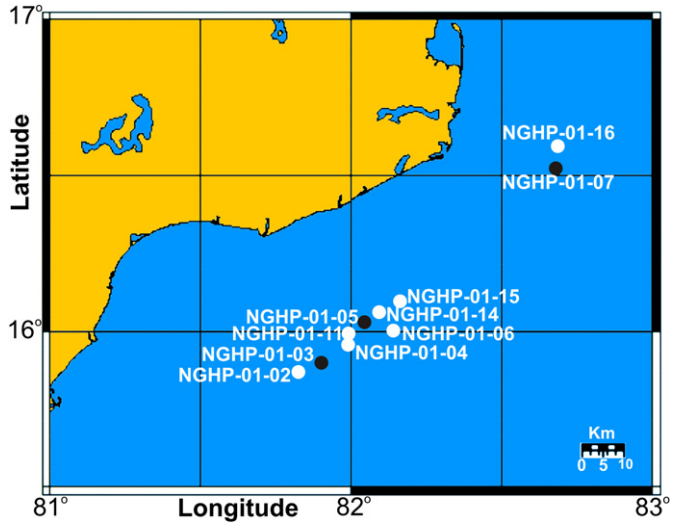

Figure 1. Map of the study area in the Krishna–Godavari Basin, eastern continental margin of India. Locations of drill sites used in this study area are shown with circles and site names.

2. Log data and methods

The down-hole logging program during NGHP Expedition 01 was specifically designed to assess the presence and saturation of gas hydrates on the continental margin of India (Collett et al., 2008a). Several LWD and wire-line logging devices were deployed, as described below. Not all tool strings were run in each hole. During NGHP Expedition 01, LWD data were acquired at five sites drilled in the KG Basin on the eastern continental margin of India.

2.1. Porosity log

Log density–derived porosities are obtained from the LWD density log by using the formation bulk density (ρ_b), the density of water (ρ_w) taken to be 1030 kg/m^3, and the average grain density (ρ_g) measured in the core MAD analysis (2750 kg/m^3) using the density porosity formula,

$$\varphi = \left(\rho_g - \rho_b\right) \Big/ \left(\rho_g - \rho_w\right) \quad (1)$$

The variance in grain density measurements yielded a standard deviation of ~ 45–100 kg/m^3. Note that for the porosity estimate to exclude bound water, the average grain density must include the clay component of the sediment matrix. A log measurement of formation electron density is obtained based on the reduction in gamma ray flux between a source and a detector on the sonde. The source (^{127}Cs) emits gamma rays into the formation, which are then Compton-scattered by electrons in the formation. A fraction of the emitted gamma rays are scattered toward a gamma ray counter on the logging tool. The ratio of received to emitted gamma rays depends on the formation electron density, which is closely proportional to the formation bulk density because of the well-known relation between atomic number and atomic mass. High concentration of certain elements with unusual electron density responses can result in error (Hearst et al., 2000); however, this is not expected to be a problem given the composition of the sediments studied.

Clay minerals, when present in large enough concentration, can contain a significant amount of bound water that is measured by the neutron porosity tool as pore space, rather than sediment matrix. For this reason, in clay-rich sediments, porosity estimates from neutron logs are generally greater than those from density porosity. The Archie analysis is first undertaken using the log density porosity. The density porosity is generally more reliable than the neutron porosity, since the calibration of neutron porosity contain additional uncertainties related to the effect of unknown

amount of hydrocarbon (including gas hydrate and free gas) on hydrocarbon concentration, and the high sensitivity of the neutron porosity measurement to hole conditions. Figure 2 shows the measured LWD porosity at three NGHP Expedition 01 sites.

2.2. Resistivity log data

Down-hole formation electrical resistivity data have been obtained from NGHP Expedition 01 using conventional wire-line and LWD logging tools. The instruments both use high-frequency alternating magnetic fields that induce secondary currents in the formation. These ground-loop currents produce new inductive signals, proportional to the conductivity of the formation. The vertical resolution of the tools is about 2 m, and the data are reasonably insensitive to variable hole diameter. Resistivity calibrations are estimated to be about ±10% of the measured resistivity (Schlumberger, 1989). A medium induction tool and a spherically focused tool provide additional resistivity data with higher spatial resolution but they are more affected by the washed-out and variable hole diameters. The most reliable down-hole resistivity measurement is obtained from the LWD GeoVISION resistivity at the bit (RAB) tool. The RAB tool is connected directly above the drill bit and uses two transmitter coils and several electrodes to obtain different measurements of resistivity. Resistivity is measured using a focusing technique: the upper and lower transmitter coils produce currents in the drill collar that meet at the ring electrode. In a homogeneous medium, a net current flow perpendicular to the tool would occur at the ring electrode. This radial current flow becomes distorted in heterogeneous formations, and the current required through the ring electrode to focus current flow into the formation is related to the formation resistivity (Collett et al., 2008a).

Figure 3 shows representative examples of the RAB resistivity profiles at three sites of the NGHP Expedition 01. At each of these sites, the seismically inferred base of gas hydrate stability zone (or BSR depth) is shown. Used alone, these resistivity logs qualitatively indicate certain zones of gas hydrate occurrence. High porosity unconsolidated marine sediments in the study area generally have resistivities on the order of 1 Ωm. Certain zones above the inferred BSR exhibit much higher resistivities and are therefore interpreted to be gas hydrate bearing, notably at site NGHP-01-03 at 170–200 m below seafloor (mbsf), at site NGHP-01-05 in thick layer 56–94 mbsf, and at site NGHP-01-07 in thin layers between 70-90 and 135–155 mbsf.

The base of the gas hydrate stability zone (BGHSZ) can be inferred from the resistivity logs by a pronounced decrease in resistivity values from 1.4 to 0.9 Ωm at site NGHP-01-03 near 200 mbsf, from ~1.4 Ωm to ~1.0 Ωm at Site NGHP-01-05 at 120 mbsf, and at site NGHP-01-07 from ~1.4 Ωm to 1.2 Ωm. Site NGHP-01-05 shows an almost constant ~1.0 Ωm resistivity below the BGHSZ (Fig. 3). Free gas immediately beneath the BGHSZ also increases the resistivity in general, explaining why no obvious decrease in resistivity at the BGHSZ may be observed at some sites. In some cases the log-defined BGHSZ is shallower than the seismically defined BSR, probably reflecting uncertainties in velocity-depth conversions.

2.3. Archie's law for electrical resistivity

Gas hydrate bearing sediments exhibit relatively high electrical resistivity values in comparison to water-saturated units, which suggest that a down-hole resistivity log can be used to identify and assess the amount of gas hydrate present within a sedimentary section. The relation between rock and pore fluid resistivity has been studied in numerous laboratory and field experiments. Many subsequent studies using borehole log data, core data and laboratory measurements have confirmed the exponential relation to be a good approximation for relating resistivity to porosity (e.g.,

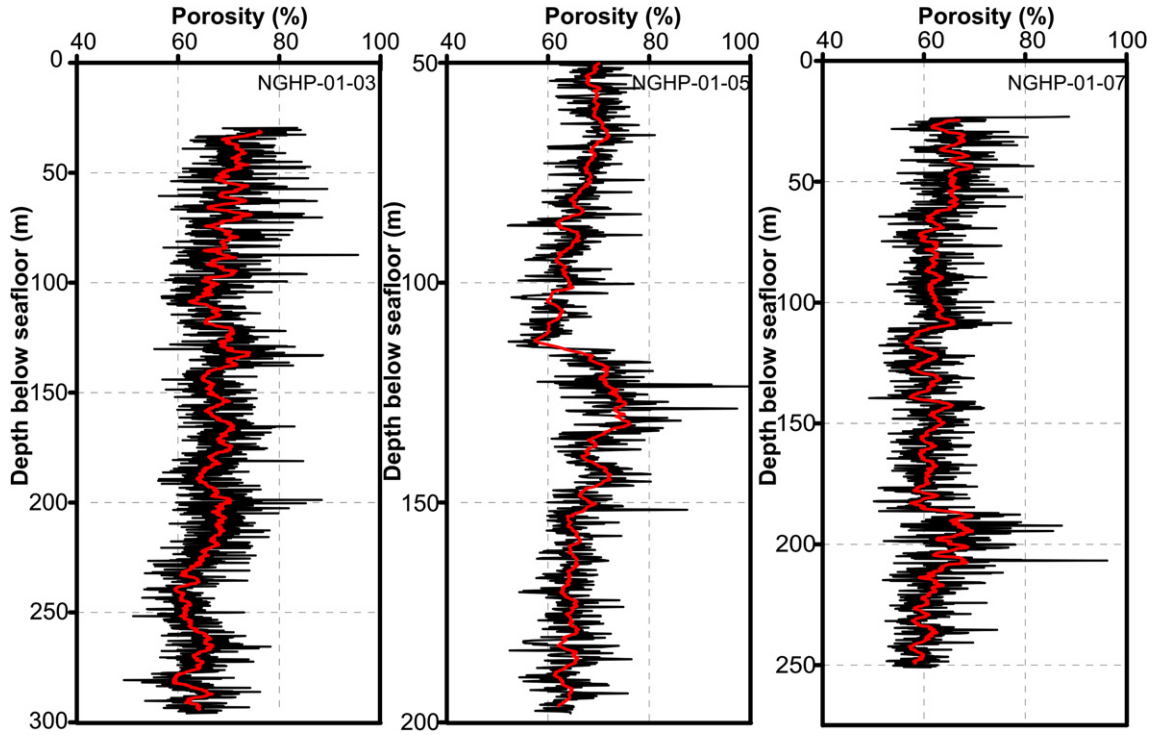

Figure 2. Down-hole Logging-While-Drilling (LWD) porosity measurements at three example sites from India National Gas Hydrate Program (NGHP) Expedition 01 (NGHP-01-03, NGHP-01-05 and NGHP-01-07). Red bold line shows the twenty point running average (For interpretation of the references to colour in this figure legend, the reader is referred to the web version of this article).

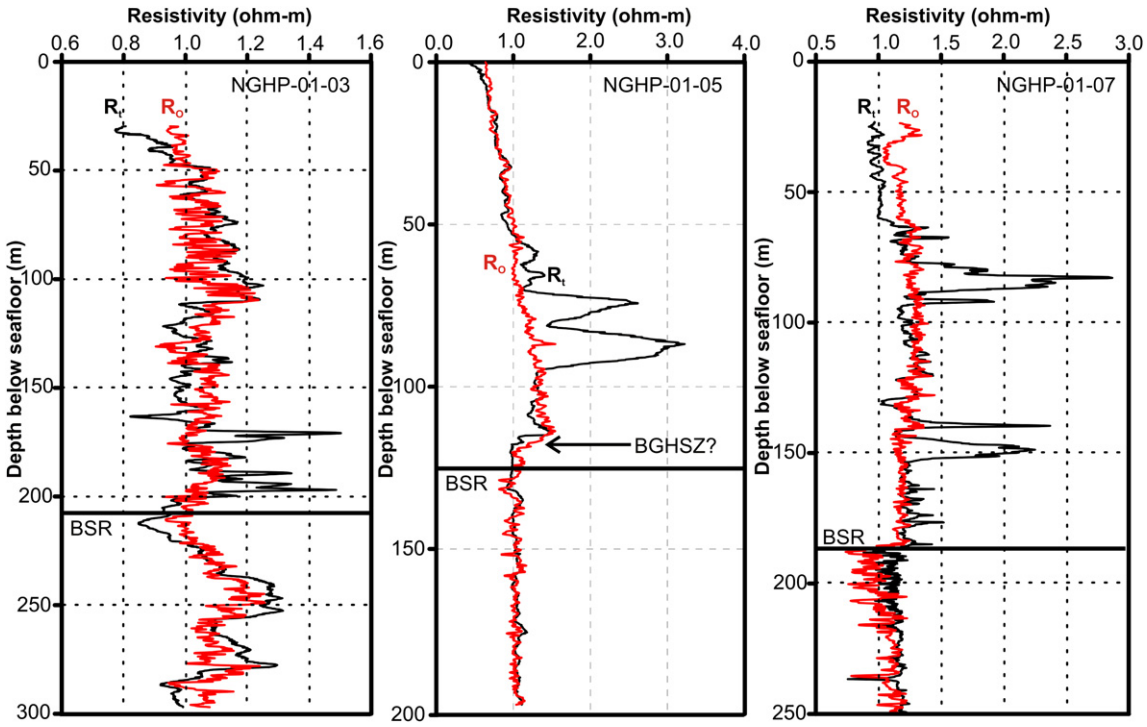

Figure 3. Measured Logging-While-Drilling (LWD) resistivity R_t (black) and 100% water-saturated resistivity R_o (red), determined from the Archie analysis of down-hole data from India National Gas Hydrate Program (NGHP) Expedition 01, at three sites of the well transect. R_o is calculated from the log density porosity. Estimates of the base of gas hydrate stability zone (BGHSZ) sometimes differ from seismically defined bottom-simulating reflector (BSR) (For interpretation of the references to colour in this figure legend, the reader is referred to the web version of this article).

Jackson et al., 1978; Swanson, 1979; Hilfer, 1991; Ioannidis et al., 1997), and adequate for the purpose of this study.

The electrical resistivity of water-saturated sediments (R_o) can be expressed using the Archie's (1942) equation as given below:

$$R_o = \left(aR_w/\varphi^m\right) \tag{2}$$

where, R_o is the formation resistivity of water-saturated sediment, R_w is the resistivity of the connate water, a and m are Archie constants, and φ is the porosity. Archie constants a and m can be derived empirically; a is Archie coefficient and m is commonly called the cementation factor. These a and m values depend on the interaction between the host sediments and gas hydrate in the porous medium. From a physical perspective, the value of parameters a and m depends on the inter-connectivity of the pore spaces, which in turn depends on lithology, cementation, and grain size distribution (Hearst et al., 2000). Smaller values of a and m are qualitatively indicative of well inter-connected pore spaces (i.e., lower R_o for a given φ and R_w). Equation (2) can be solved for the ratio of water-saturated sediment resistivity and connate water resistivity gives formation factor (i.e. $F = R_o/R_w = a\varphi^{-m}$). The gas hydrate saturation (S_h) in the formation from the resistivity log data can be estimated from Archie's (1942) equation given below.

$$S_h = 1 - \left(aR_w\varphi^{-m}/R_t\right)^{1/n} \tag{3}$$

2.4. Determination of Archie parameters

To make a quantitative estimate of the amount of gas hydrate using electrical resistivity log data we apply the Archie relationship to the resistivity and porosity logs recorded at 10 sites in the KG Basin including Site NGHP-01-02, -03, -04, -05, -06, -07, -11, -14, -15, and -16 (see summary of values in Table 1). By using the

Table 1
Archie's constants (a and m) derived from pickett plots for the 10 sites in the KG Basin, and average gas hydrate saturation for entire gas hydrate stability zone. Sites NGHP-01-02, -04, -06, -11 were determined using Arp's formula. All other sites are based on estimates of the *in situ* pore-water resistivity using the equation of state of seawater by Fofonoff (1985) (Values denoted by asterisk have been adjusted for fracture-filling gas hydrates, details see text).

Site	Seafloor Temperature	Geothermal gradient (°C/km)	BGHSZ (mbsf)	Hydrate Bearing Zone (mbsf)	Archie constants		Average S_h	Pickett plot R^2 value
					a	*m*		
NGHP-01-02	6.5	45	170	–	2.02	1.35	0.002	0.80
NGHP-01-03	6.5	39	209	170–200	2.27	0.98	0.02	0.60
NGHP-01-04	6.7	42	182	82–100	1.63	1.69	0.012	0.73
NGHP-01-05	7.1	44	125	56–94	2.23	1.12	0.023*	0.84
NGHP-01-06	7.9	37	210	106–210	1.80	1.48	0.044	0.80
NGHP-01-07	5.2	52	188	70–90/135–155	1.91	1.16	0.046*	0.77
NGHP-01-11	6.7	42	150	98–113	1.55	1.61	0.023	0.77
NGHP-01-14	7.9	38	109	83–86/90–97	2.29	1.20	0.01	0.77
NGHP-01-15	7.7	40	126	70-89/90-104	3.37	0.58	0.034	0.53
NGHP-01-16	5.9	52	170	61–79/90–154	3.34	0.31	0.10	0.41

Archie's (1942) law, sediment bulk electrical resistivity for purely (saline) water-saturated sediments can be calculated by equation (2). However, we calculated R_w using the equation of state of seawater (Fofonoff, 1985). Pressure is taken to be hydrostatic, *in situ* temperature measurements, core-salinity measurements at the same site and geothermal gradient constrained from the NGHP Expedition 01 are utilized to derive the resistivity of connate water. Figure 4 shows the pore-water resistivity versus depth profiles derived from the core-salinity, seafloor temperature, and geothermal gradient for Sites NGHP-01-03, -05, and -07. Solid lines represent the smooth linear fit for the interpolation of the R_w using linear fit regression equations for the respective sites. The calculated R_w from the measured salinity and temperature along with estimated electrical resistivity for the three NGHP drill sites shows slightly decrease in resistivity with the depth below seafloor. We utilize density porosity in all the outlined calculations. Empirical Archie parameters a and m can then be estimated from a cross-plot of formation factor (F) and density porosity (φ) (Pickett plot) for sediments containing no gas hydrate (Fig. 5). Gas hydrate–free zones are chosen from the different holes, where little or no gas hydrate was interpreted (i.e. no large spikes in resistivity logs are observed).

On Figure 3 the difference between the calculated *in situ* resistivity (R_o) and measured log resistivity (R_t) for the three sites used as representative examples can be clearly observed. This figure demonstrates that the calculated R_o agrees well with the measured resistivity for most intervals; however the calculated R_o is higher than the measured resistivity where significant amount of shale (clay) exists. This implies that the clay effect on resistivity may be significant at the KG Basin wells, partly because of the high resistivity of the connate water itself.

In the absence of core-derived *in situ* pore-water salinities and geothermal measurements, we invoke Arps' (1953) formula to define the *in situ* pore-water resistivity:

$$R_1(T_1 + 21.5) = R_2(T_2 + 21.5) \quad (4)$$

where R_1 is a known resistivity at temperature T_1. We used seawater resistivity at the seafloor of salinity 34 ppt, and seabottom temperatures as defined from empirical relationships by Shankar et al. (in press) to define R_1. Geothermal gradients are derived from empirical relationships by Shankar et al. (in press) to estimate the down-hole trend in R_w. The main limitation in this approach is the assumption of constant pore-water salinity trends with depth (here we use 34 ppt). However, only minor variations in the pore-water salinity were encountered during the drilling with most sites cored showing 34 + 1.5 ppt down-hole (Collett et al., 2008a), and only negligible freshening trends were seen, excluding the induced freshening from gas hydrate dissociation upon core recovery. Using the Arps' (1953) formula allowed us to augment the data base of resistivity-based gas hydrate saturation estimates by including Sites NGHP-01-02, -04, -06, and -11, all of which have LWD data but were not selected for additional coring.

2.5. Sonic log data

The LWD Sonic VISION tool was used during the India NGHP Expedition 01. The tool records monopole acoustic waveforms (13 kHz) at four receiver locations above the source along the tool string (at 3.05, 3.25, 3.45, and 3.65 m distance). LWD sonic measurements are affected by the drilling noise. Therefore consecutive waveforms are stacked (on average eight) to increase the signal-to-noise ratio. The sonic tool must also be kept centralized in the borehole to maximize the signal strength. Down-hole velocity data were also measured by WL logging with the dipole sonic imager (DSI) tool; however, typically the drill-string is lowered into the formation by ~50–60 m, thus limiting the depth interval of available data. The DSI measures P- and S-wave transit times between a sonic transmitter and an array of eight receiver

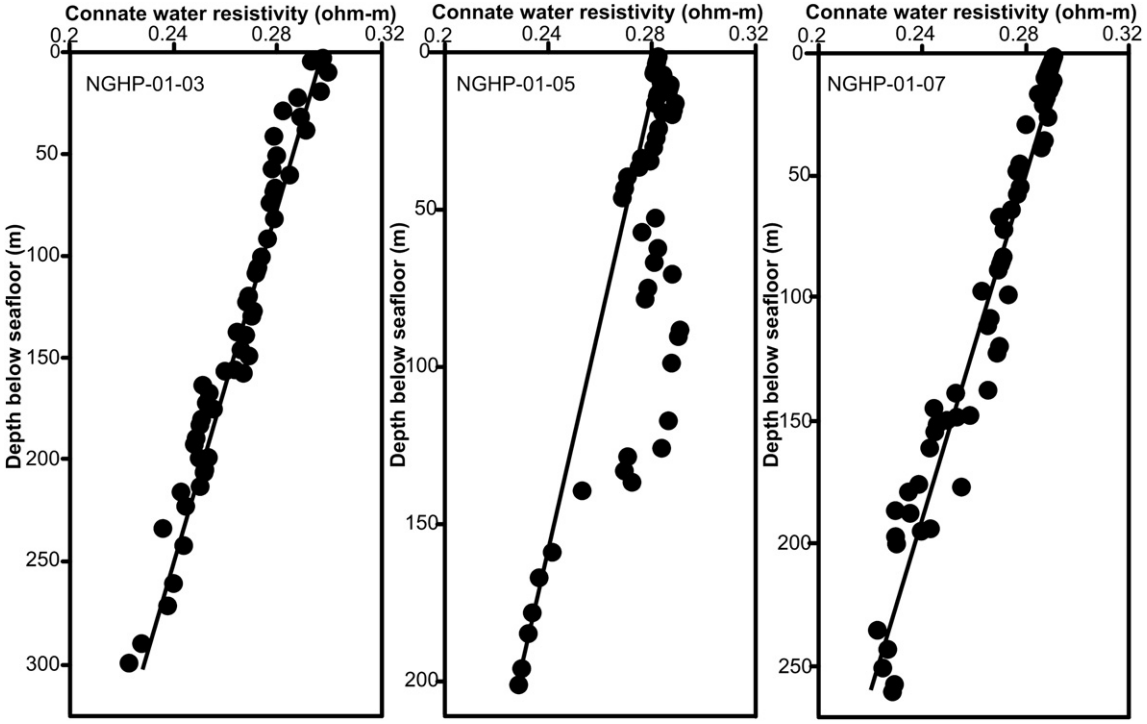

Figure 4. Calculated resistivity of connate water (R_w) at three India National Gas Hydrate Program (NGHP) Expedition 01 sites (NGHP-01-03, NGHP-01-05 and NGHP-01-07) with measured temperature and salinity using Fofonoff (1985) equation of state for seawater. Solid bold line shows the best linear fit .

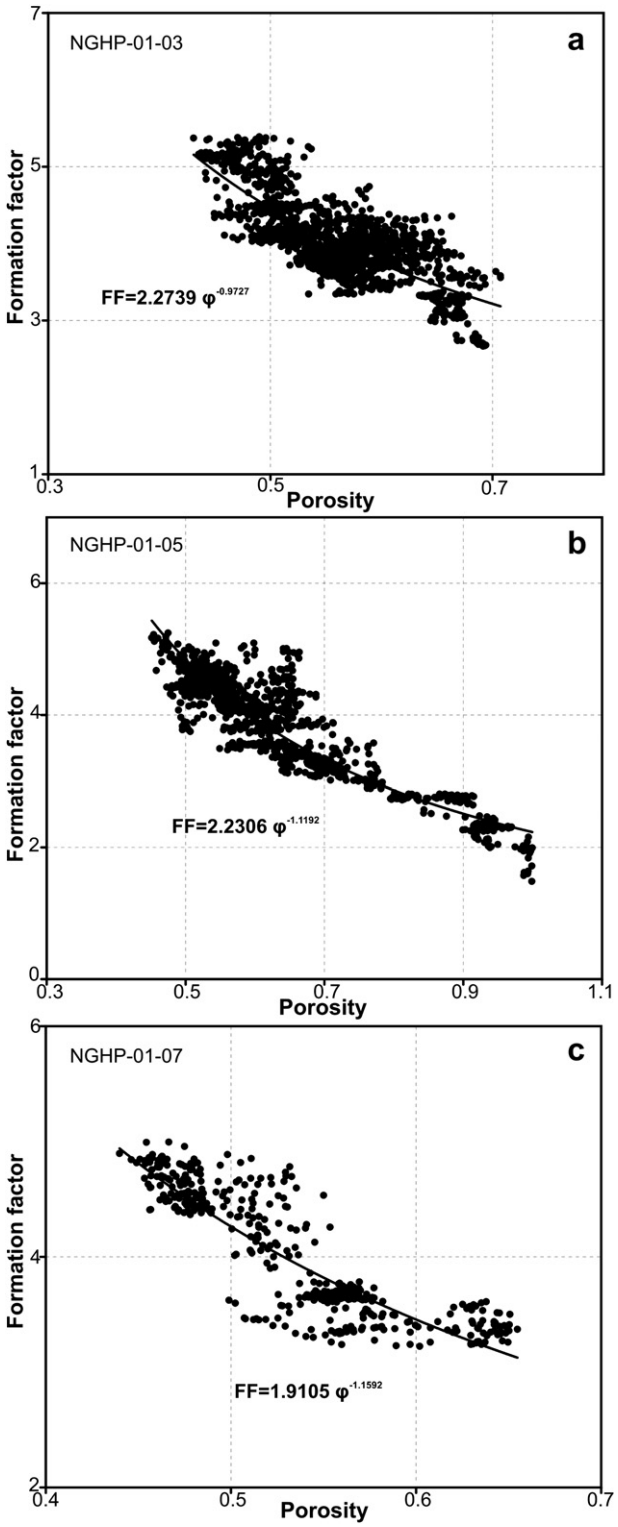

Figure 5. Formation factor (FF) is plotted versus porosity (Pickett Plot) for (a) site NGHP-01-03, (b) Site NGHP-01-05, and (c) Site NGHP-01-07. The data points are all taken from non-hydrate bearing sediments and sub-BSR zones. The bold solid line is the best exponential fit, giving Archie's parameters, which are summarized in Table 1.

groups at 15 cm spacing. P- and S-wave transit times (slowness) are used to compute P- and S-wave velocity, with the data processing done in real time. The vertical resolution of the tool is 107 cm, and the depth of investigation is ~10 cm. The hole size calculated from the caliper log shows an irregular hole, with alternating washouts and ledges where the hole can be smaller than the bit size. Despite the irregular size the quality of the data should be only moderately affected. An indication of the general good data quality is the good agreement between the density log and the core measurements. While this naturally coincides with a good agreement between the porosity measurements on core samples and the density–derived porosity log, the neutron porosity log indicates larger values due to the bound clay water. This difference is due to the large hole in some intervals, but it is mainly related to the large amount of clay in this formation, which is not corrected for in the neutron porosity log. The quality of the sonic log is highly dependent on borehole conditions, and requires good contact between the tool and the borehole wall. The quality of the sonic logs is therefore good (Collett et al., 2008a). P-wave velocities for three sites from NGHP Expedition 01 sonic logs are shown in Figure 6.

2.6. Rock-physics modeling

An alternative approach to empirical porosity–velocity relations and time-averaging is to derive bulk sediment elastic properties from a rock-physics model (e.g., Dvorkin and Nur, 1993; Carcione and Tinivella, 2000; Helgerud et al., 1999). A comparison of theoretical methods, including various rock-physics models is given by Chand et al. (2004). The rock-physics model used in this study is that of Helgerud et al. (1999), developed for high porosity clay-rich marine sediments.

The approach of Helgerud et al. (1999) was to build a first-principles-based effective medium model for the elastic moduli of high porosity marine sediments containing gas hydrate or free gas. The model requires knowledge of the porosity and of the elastic moduli of the sediment constituents: gas hydrate, free gas, the pore-water, and the sediment grains. A baseline model for fully water-saturated sediments developed by Dvorkin et al. (1999) is used as a starting point. The sediment matrix is modeled as packed spheres, each with 8 grain contacts. The elastic properties of the effective medium composed of the fully water-saturated sphere pack is then calculated from first principles. Applied to a sediment column with known mineral constituents and known porosity–depth profile, this model gives a baseline no-hydrate velocity-depth profile. However, it is relatively sensitive to the mineral assemblage chosen in the modeling.

Elastic properties of effective media containing various amounts of gas hydrate or free gas can then be calculated, according to different assumptions concerning their formation mechanisms (Helgerud et al., 1999). Gas hydrate is modeled either as part of the pore fluid (gas hydrate in-pore), or as part of the load-bearing sediment matrix (gas hydrate in-frame). The gas hydrate in-pore model assumes that the gas hydrate occurs in the sediment pore space, without adding stiffness to the sediment frame. As a consequence, the sediment S- (shear) wave velocity is nearly unaffected by the occurrence of gas hydrate. For the gas hydrate in-frame model, elastic properties of the sediment frame are recalculated, with grains of gas hydrate included as part of the sediment frame. Under this mode of occurrence, gas hydrate adds some stiffness to the sediment frame, and the sediment S-wave velocity is slightly increased by gas hydrate but much less so than for a model in which gas hydrate cements the grain contacts (e.g., Dvorkin and Nur, 1993). Both the gas hydrate in-pore and in-frame models predict an increase in P-wave velocity with increased gas hydrate saturation (slightly more for the gas hydrate in-frame model). Application of this effective medium model to down-hole VSP data from ODP Leg 164 Hole 995 at the Blake-Bahama Ridge gas hydrate site indicated that the gas hydrate in-frame model is most accurate in high porosity clay-rich marine sediments (Helgerud et al., 1999).

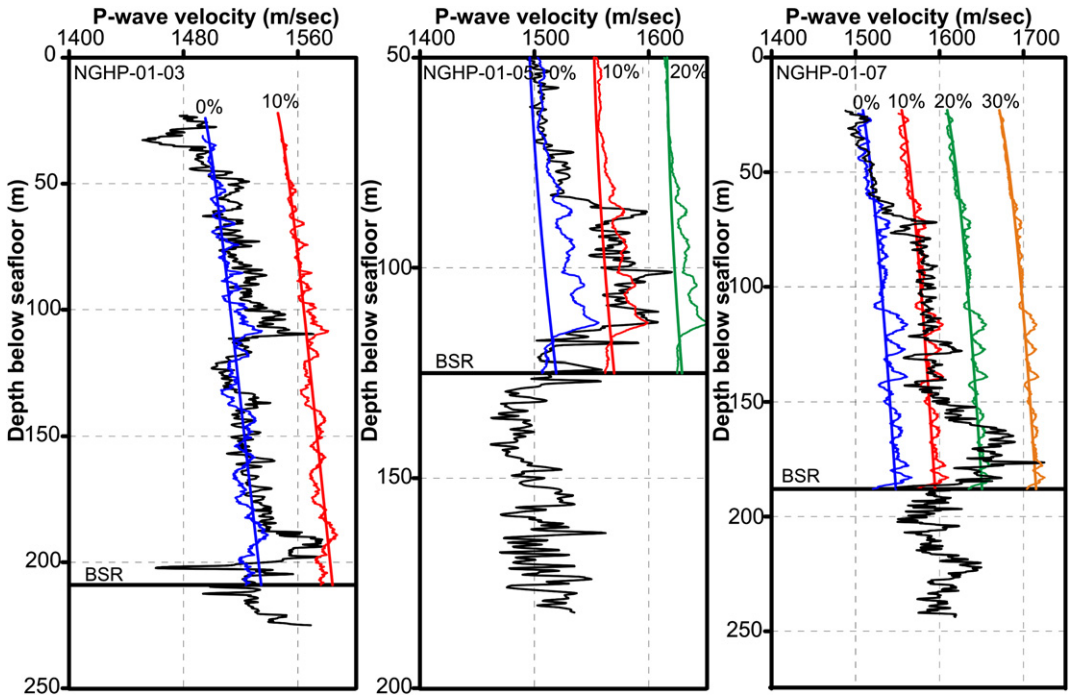

Figure 6. P-wave velocity measurements from LWD logs and predicted velocities for gas hydrate bearing sediments using the gas hydrate in-frame rock-physics model for varying gas hydrate saturations at the three Sites NGHP-01-03, -05, and -07 (from left to right). Straight lines are based on smoothed porosity trends, whereas a twenty point running average was also used to achieve higher resolution in the prediction.

3. Gas hydrate saturation (S_h) estimation from logs

There is an extensive body of literature on the use of well logs for estimating gas hydrate saturations (e.g., Collett et al., 1984, 1999; Collett, 2001; Collett and Lee, 2004; Kleinberg et al., 2003, 2005; Lee and Collett, 2008; Mathews, 1986; Guerin et al., 1999, Hyndman et al., 1999). The most commonly used logs for gas hydrate saturation estimates include resistivity and sonic logs. Below, we discuss the gas hydrate saturation estimates based on resistivity and sonic measurements at the three example NGHP Expedition 01 sites (NGHP-01-03, -05, and -07).

3.1. Gas hydrate saturation from resistivity

With the empirically estimated Archie parameters *a, m,* and *n,* equation (3) can be used to calculate S_h. Gas hydrate saturation estimates from electrical resistivity logs are sensitive to *n* at higher gas hydrate saturations. From a physical perspective, choosing a value for *n* similar to that of *m* implies the assumption that the effect of gas hydrate formation on the electrical resistivity is similar to that of simple effective porosity reduction. Pearson et al. (1983) calculated an estimate for *n* of 1.94; however, modeling by Spangenberg (2001) has shown that *n* depends somewhat on grain size distribution and the gas hydrate saturation itself. We used ($n = 1.94$) for our estimates.

Down-hole profiles of gas hydrate saturation (S_h) from resistivity at the three sites are shown in Figure 7. Two zones in the interval from 70 m to 90 m, with S_h-values almost at 38% are seen at site NGHP-05. Site NGHP-03 shows gas hydrate saturations that are overall less than 10% with few thin intervals showing saturation reaching up to 20%. At site NGHP-07 gas hydrate saturation is up to 30% in two intervals from 25 m to 40 m and 145 m–153 m (Fig. 7). The average gas hydrate saturation estimated from all ten sites using resistivity logs are given in Table 1. A discussion on effects from fracture-filling gas hydrate on the resistivity-based saturations is given below.

3.2. Gas hydrate saturation using rock-physics modeling

At each well site, a reference velocity-depth profile is calculated from the Helgerud et al. (1999) rock-physics model to match the observations in the measured LWD velocity logs. Two porosity trends are adopted: one is the smoothed linear fit and the other a 20 point running average porosity–depth profile. The averaging mineralogy is taken to be 90% clay and 10% quartz, with the elastic parameters of the sediment constituents summarized in Table 2. To estimate gas hydrate saturation, P-wave velocity vs. depth profiles for various gas hydrate saturations are computed, using the gas hydrate in-frame model. These constant gas hydrate saturation profiles are plotted with measured P-wave velocity data to provide an estimate of gas hydrate saturation.

Figures 6 shows gas hydrate saturation estimates from the gas hydrate in-frame rock-physics models, estimated from P-wave velocity data for the three NGHP Expedition 01 example sites. Estimates from the rock-physics modeling are in overall agreement with result from the electrical resistivity approach; however, results from velocity modeling show a tendency to slightly higher average values (Table 3). P-wave velocity data at site NGHP-01-03 predicts gas hydrate saturation of maximum 10%. In the high S_h area at site NGHP-01-05 starting from depth around 70 mbsf up to the BSR depth is more than 10% and less than 20%. At site NGHP-01-07 estimated gas hydrate saturation are over 10% (starting at ~70 mbsf) and saturation increases from depth 150-188 mbsf up to 20% (Fig. 6).

4. Regional gas hydrate volume assessment

In this exercise we attempted to estimate the total amount of gas hydrate in the study area of the KG basin, which can be used later as

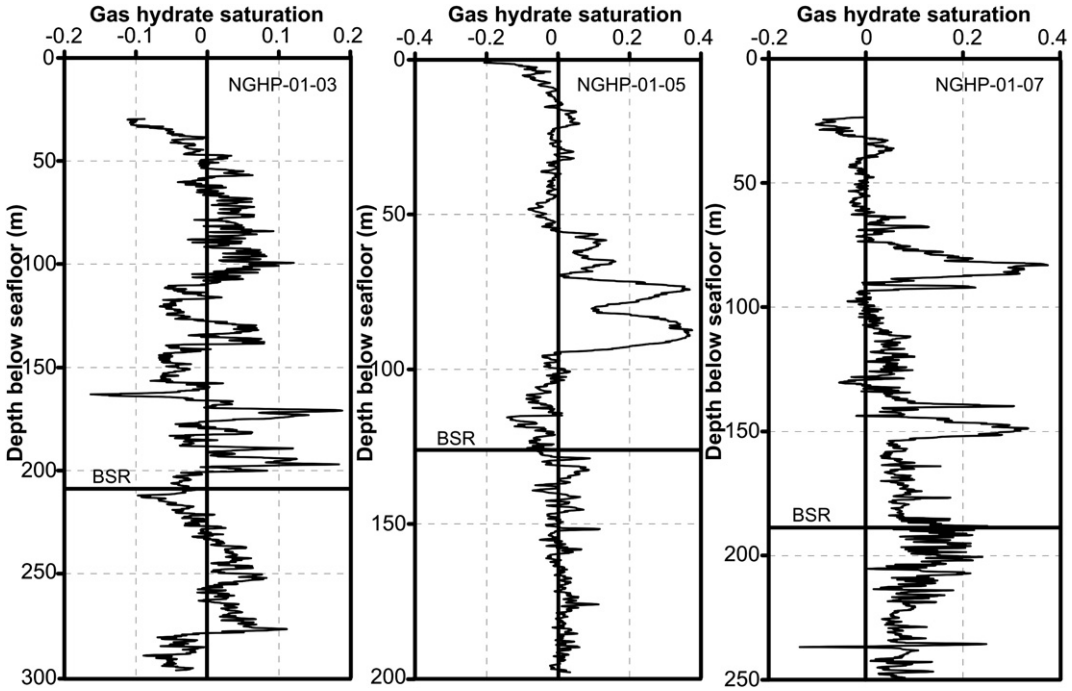

Figure 7. Gas hydrate saturation estimates from resistivity log using Archie analysis for the three sites of the NGHP Expedition 01 well transect, calculated using the log density porosity method. Values below BSR are not representing gas hydrate saturations.

key ingredient in other studies related e.g. to carbon cycles and climate change. We base the calculations on the assumption that we only find structure-I gas hydrate, as the drilling showed that 99.9% of the gas recovered (in voids and from gas hydrate samples) is biogenic methane (Collett et al., 2008a).

The first step in this calculation is the definition of the areal extent of gas hydrate occurrence. We base this on seismic observations of the BSR (Fig. 8), acknowledging that this may result in an overall conservative estimate, as the absence of a BSR does not necessarily mean an absence of gas hydrate. However, conversely, the presence of a BSR does indicate the presence of gas hydrate. But the BSR in itself does not provide information on how much gas hydrate may be present and where it is located within the gas hydrate stability zone. Using the distribution of BSRs in the 2D and 3D seismic data (Fig. 8) we define the areal extent of gas hydrate occurrence to ~720 km^2. The vertical extent of the gas hydrate stability zone (GHSZ) can be calculated from the depth of the BSR and transforming the observed travel-times to meter below seafloor (mbsf) using seismic velocity. An average velocity of 1580 m/s was used based on the available sonic log data and the average thickness of the gas hydrate stability zone below seafloor is 177 m. This yields a total volume of $\sim 1.27 \times 10^{11}$ m^3 of sediments.

Porosity logs from the 10 sites investigated show that porosity is typically ranging between values near ~70% at the seafloor to ~55% around the depths of the BSR (Fig. 2). An average of 60% (±5%) can therefore be assumed for further calculations.

When combining gas hydrate saturation (S_h) with estimates of the thickness of the gas hydrate stability zone (which is basically the thickness between seafloor and the BSR) an average gas hydrate saturation for the same thickness needs to be defined. However, our data are in most cases incomplete, as reliable log data are not available for the entire zone of interest, and on average good-quality logs start at ~30 mbsf for LWD, and below the casing set for wire-line logging (50–60 mbsf). We therefore fill in the missing log-intervals and in all cases we replaced the missing intervals with $S_h = 0$. While this is likely valid for the LWD log data cases, where the missing interval is the shallowest interval (top 30 mbsf), and no gas hydrate is expected here, this cannot be necessarily assumed for the wire-line log data cases (Sites NGHP-01-14, -15, -16), where gas hydrate may be occurring within the interval occupied by the drill-pipe. In such case we verified the absence of gas hydrate using available gas hydrate proxies from the core data, i.e. presence of Infra-red anomalies, mousse-like textures of the sediments, and pore-water freshening. All gas hydrate saturation estimates based on electrical resistivity and P-wave velocity from all Sites used in this study are summarized in Tables 1 and 3. If gas hydrates saturations from both, resistivity and P-wave velocity are available, the two values are combined for the site and one average S_h-value is used for further calculations. Finally all gas hydrate saturation estimates at all 10 Sites are averaged, yielding a value of 4.05% of the pore spaces. The total amount of gas hydrate (TGH) can now be calculated:

Table 2
Elastic properties of sediment constituents (After Helgerud et al., 1999).

Sediment Constituents	Bulk Modulus (GPa)	Shear Modulus (Gpa)	Density (g/cm^3)	P-wave Velocity (km/s)	S-wave Velocity (km/s)
Clay	20.9	6.85	2.58	3.41	1.63
Quartz	36.6	45.0	2.65	6.04	4.12
Pore-Water	2.4	0.0	1.03	1.5	0.0
Methane Hydrate	8.7	3.5	0.92	3.8	2.0
Methane gas	0.1245	0.0	0.25	0.71	0.0

Table 3
Average gas hydrate saturation for entire gas hydrate stability zone for various NGHP sites from rock-physics model.

Site	Logged	BGHSZ (mbsf)	Hydrate occurring zone (mbsf)	Average S_h
NGHP-01-02	LWD	170	118–160	0.03
NGHP-01-03	LWD	209	99–109,188–197	0.043
NGHP-01-04	LWD	182	112–131, 150–182	0.027
NGHP-01-05	LWD	125	85–114	0.028
NGHP-01-06	LWD	210	64–80, 168–191	0.077
NGHP-01-07	LWD	188	70–77, 124–129, 160–188	0.093
NGHP-01-11	LWD	150	111–150	0.033
NGHP-01-14	WL	109	70–109	0.026
NGHP-01-15	WL	126	65–126	0.048
NGHP-01-16	WL	170	60–80, 90–120	0.089

$$\mathrm{TGH} = \mathrm{Area} \times \mathrm{GHSZ} \times \mathrm{Porosity} \times S_h\,, \tag{5}$$

with an area of 720 km^2, a thickness of the GHSZ of ~177 m, an average porosity of 60% and an average S_h of 4.05%, the total amount of gas hydrate is ~3.1×10^9 m^3. Converting this to the amount of gas, we use a volume-change factor of 164 and get ~5.08×10^{11} m^3 of gas (equivalent to ~17.94 trillion cubic feet, TCF). Porosity may change by ±5% and the standard deviation for the average gas hydrate saturation is ~2.65%. Thus the total amount of gas hydrate may vary from ~9.8×10^8 to ~5.6×10^9 m^3 (or equivalent ~5.7 to ~32.1 TCF of gas).

5. Discussions

The presented gas hydrate saturation estimates are based on several assumptions, where the most fundamental assumption is the mode of gas hydrate occurrence as pore-filling medium (effectively reducing porosity, without adding stiffness to the overall sediment matrix or cementing the individual sediment constituents) so that Archie's (1942) relationship and an effective medium model can be invoked in the calculations. From the 10 drill sites selected, Sites NGHP-01-05 and NGHP-01-07 have a different mode of gas hydrate occurrence in dominantly fracture-filling form (Collett et al., 2008a; Lee and Collett, 2009; Cook and Goldberg, 2008a, b). It has been shown that in case of fracture-dominated gas hydrate occurrence, the standard Archie analysis overestimates the gas hydrate saturation (Lee and Collett, 2009). We derived gas hydrate saturations as high as 38% of the pore space for intervals at Site NGHP-01-05 and -07 (Fig. 7) that had considerable amounts of fracture-filling gas hydrate. It should be noted that the P-wave velocity logs at both sites do not show the same structure with elevated velocities in certain intervals that would yield artificially high gas hydrate saturations. This is likely due to the geometry of the LWD velocity tool not being as receptive to the anisotropy imposed by the fractures as the resistivity tool. Using the recovered pressure cores from these intervals of fracture-filling gas hydrate as a reference for gas hydrate saturations it is possible to downscale the resistivity-based estimates. In case of Site NGHP-01-05, gas hydrate saturations derived from pressure cores are maximum 9.4% (of pore-volume) for the fracture-dominated intervals (about one quarter to a third of the log-derived estimates). This factor (0.25–0.33) between Archie-based and pressure core-derived saturation estimates is very similar to observations made by Lee and Collett (2009) at Site NGHP-01-10. However, some care must be taken in the comparison: Pressure cores are typically 1 m long (often less) with a diameter of 4.3 cm and thus represent only a small portion of the gas hydrate interval tested. Also, pressure core recovery is not always successful, giving an incomplete picture of the *in situ* conditions. While these pressure core-derived saturations are very accurate, they may also represent the low-end of possible values. However, in order to account for violating the assumption of pore-filling gas hydrate and using Archie's (1942) law, and thus overestimating the saturations, we weighted the intervals of fracture-filling gas hydrate at Site NGHP-01-05 and NGHP-01-07 with a factor of 0.3. This resulted in a reduction for the resistivity-based average S_h-value from 6.1% to 2.3% at Site NGHP-01-05 and from 5.7% to 4.6% at Site NGHP-01-07 (Table 1). In comparison, average S_h from velocity modeling at Site NGHP-01-05 yielded a saturation of 2.8% and at Site NGHP-01-07 a saturation of 9.3%. We also want to note that we excluded Site NGHP-01-10 from the calculations as this site is very unusual for the KG Basin. At Site NGHP-01-10 the entire gas hydrate occurrence zone is fracture-dominated and probably this site was a cold-vent in geologic history as suggested by the presence of buried chemo-synthetic communities (Collett et al., 2008a; Mazumdar et al., 2009). Estimates of gas hydrate saturations based on the log-properties have already been shown as heavily biased to too high values by Lee and Collett (2009) who introduced a modeling approach incorporating anisotropy. However, conditions as at Site NGHP-01-10 have not been encountered anywhere else during the drilling expedition, thus it is not meaningful to include this area into the overall volume estimate.

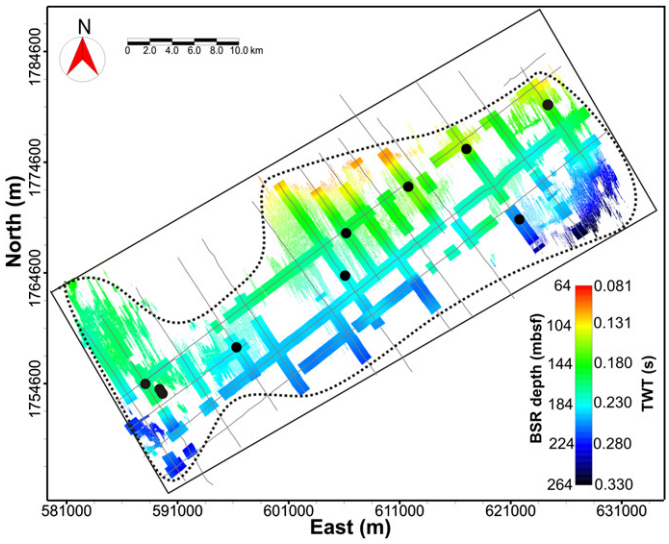

Figure 8. Observed BSR depth distribution from 2D and 3D seismic lines. The color bar represents depth of BSR below seafloor in two-way time (TWT, in sec) and meters, respectively. Dotted outlined area (~720 km^2) was used for volume estimation (For interpretation of the references to colour in this figure legend, the reader is referred to the web version of this article).

Additional uncertainties in the resistivity-based S_h-value arise from the methodology itself, i.e. the Pickett plot analysis to derive empirical Archie parameters a and m, as well as the assumed value of n. In part these uncertainties are quantified by the R^2 value of the fit of Archie's (1942) relation to the data (Fig. 5, Table 1). A different approach to the Pickett plot analysis was used during the India NGHP expedition to estimate gas hydrate saturation onboard (Collett et al., 2008a), where the Archie coefficient a is held constant at 1.0, and only m is being defined statistically from the data. Both approaches yield on average the same saturations.

The main source of uncertainty in gas hydrate saturation estimates from the rock-physics modeling approach is related to the choice of the mineral assemblage used to build the model, and the elastic properties of those mineral components. We based our choices on the sedimentological descriptions of the recovered core. The fact that our baseline of '0'-gas hydrate follows closely the measured P-wave velocity in the intervals where no gas hydrate

was encountered (especially when using a 20 point average for the porosity, Fig. 6) increases our confidence in the derived gas hydrate saturation estimates from this technique.

Calculation of the total amount of gas hydrate in any given area is always challenging because of the many assumed parameters required. While linking the area of gas hydrate and the thickness of the stability zone to the occurrence of a BSR appears favorable (the presence of a BSR always indicates gas hydrate), this approach is conservative. Areas without a BSR are not necessarily hydrate-barren. Also, gas hydrate has been seen to be favorably within the sandy sections of sediments and also can occur strata bound, instead of pervasively spread out homogenously in the pore space of the sediment. Without a detailed seismic-based inversion (e.g. by Dai et al., 2008; Riedel et al., 2009) and close links between the logs and seismic events (e.g. specific sand layers), the only approach is to capture all uncertainties and define statistically meaningful extreme values. The resulting total amount of gas hydrate varies from 9.8×10^8 to 5.6×10^9 m^3 (or equivalent 5.7 to 32.1 TCF of gas) in our study area. The value can be meaningful for modeling studies looking into carbon cycles or impacts on climate change on gas hydrate dissociation. In terms of a resource assessment, the values provided by this study for the KG basin are probably less meaningful as they are pure "in place" estimates and not tied to a given reservoir (defined geologically) and a production technology. Regional assessments incorporating local geology (e.g. amount of sand occurrence) and gas hydrate production technology have been conducted for other areas such as the North Slope of Alaska (Collett et al., 2008b) and the Gulf of Mexico (Frye et al., 2008). However, these assessments are based on a larger drilling data set and a larger amount of seismic data.

6. Conclusions

We have used available logging data from the India NGHP Expedition 01 to derive estimates of gas hydrate saturation at 10 sites within the KG basin (NGHP-01-02, -03, -04, -05, -06, -07, -11, -14, -15, -16). We also used available 2D and 3D seismic data to calculate the total amount of gas hydrate present in the study area.

Gas Hydrate saturations were estimated using electrical resistivity and P-wave velocity logs. Resistivity logs were analysed using Archie's (1942) relation, combined with core-derived trends for *in situ* pore-water salinity and measurements of geothermal gradients. In the absence of core-derived measurements of these parameters, we used Arps' (1953) formula to derive *in situ* pore-water resistivity. We found that the Arps' (1953)-method reproduced reasonably well the down-hole trends in resistivity when compared to those derived from actual core measurements. Gas hydrate saturation from electrical resistivity can, however, be biased if gas hydrate does not occur in a pore-filling mode. At two sites, gas hydrate occurs as dominantly fracture-filling and thus resistivity-based estimates are too large. We used results from pressure cores to downscale the hydrate saturations for the intervals of known fracture-filling by a factor of 0.3 (empirically defined by comparing pressure core results with log-based values of hydrate saturation).

In order to estimate gas hydrate saturation from P-wave velocity, we used an effective medium modeling approach, defining average mineral assemblages based on sedimentological core descriptions, and using density porosity as input parameters. In general P-wave velocity and electrical resistivity-based approaches yield similar gas hydrate saturations.

A first attempt to a regional assessment of gas hydrate in the KG basin yields a range of total gas hydrate from $\sim 9.8 \times 10^8$ to $\sim 5.6 \times 10^9$ m^3 (or equivalent $\sim$5.7 to $\sim$32.1 TCF of gas) in our study area. This is based on a regional area estimate of $\sim$720 km^2 (where a BSR was found in 2D and 3D seismic data), average thicknesses of the gas hydrate stability zone (BSR depth), average porosities (55%–65%) and average gas hydrate saturations ($S_h = 0.0405 \pm 0.0265$) from the log analyses at 10 sites.

Acknowledgements

Authors would like to thank DGH and ONGC for their fruitful collaboration, especially by making the 2D and 3D seismic data set available for extended studies on gas hydrate in the KG Basin. We further would like to acknowledge the entire onboard team of scientists and crew-members of the India NGHP Expedition 01, who acquired the log and core data used in this analysis. In addition, U Shankar is grateful to the Department of Science and Technology, Govt. of India, New Delhi for the BOYSCAST Fellowship, 2008–2009. This is ESS Contribution number 20100037.

References

Archie, G.E., 1942. The electrical resistivity log as an aid in determining some reservoir characteristics. Trans. Am. Inst. Min., Metall. Pet. Eng. 146, 54–62.
Arps, J.J., 1953. The effect of temperature on the density and electrical resistivity of sodium chloride solutions. Petr. Trans. AIME 198, 327–330.
Carcione, J.M., Tinivella, U., 2000. Bottom-simulating reflectors: seismic velocities and AVO effects. Geophysics 65, 54–67.
Chand, S., Minshull, T.A., Gei, D., Carcione, H.M., 2004. Elastic velocity models for gas-hydrate-bearing sediments – a comparison. Geophys. J. Int. 159, 573–590.
Collett, T.S., Godbole, S.P., Economides, C.E., 1984. Quantification of in-situ gas hydrates with well logs. Proc. Annu. Tech. Meet. Petrol. Soc. CIM 35, 571–582.
Collett, T.S., Lewis, R.E., Dallimore, S.R., Lee, M.W., Mroz, T.H., Uchida, T., 1999. Detailed evaluation of gas hydrate reservoir properties using JAPEX/JNOC/GSC Mallik 2L-38 gas hydrate research well downhole well-log displays. Geol. Surv. Can. Bull. 544, 295–311.
Collett, T.S., Ladd, J., 2000. Detection of gas hydrate with downhole logs and assessment of gas hydrate concentrations (saturations) and gas volumes on the Blake Ridge with electrical resistivity data. Proc. Ocean. Drill. Prog. Sci. Results 164, 179–191.
Collett, T.S., 2001. A review of well-log analysis techniques used to assess gas-hydrate-bearing reservoirs. In: Paull, C.K., Dillon, W.P. (Eds.), Natural Gas Hydrates: Occurrence, Distribution, and Detection. Geophys. Monogr, vol. 124, pp. 189–210.
Collett, T.S., 2002. Energy resource potential of natural gas hydrates. AAPG Bull. 86 (11), 1971–1992.
Collett, T.S., Lee, M., 2004. Archie well log analysis of gas hydrate saturations in the Mallik 5L-38 well. In: Dallimore, S.R., Collett, T.S. (Eds.), Scientific Results from the Mallik 2002 Gas Hydrate Production Research Well, Mackenzie Delta, Northwest Territories, Canada. Geological Survey of Canada Bulletin, vol. 585.
Collett, T.S., Riedel, M., Cochran, J.R., Boswell, R., Presley, J., Kumar, P., Sathe, A.V., Sethi, A., Lall, M., Sibal, V., NGHP expedition 01 Scientists, 2008a. National Gas Hydrate Program Expedition 01 Initial Reports. Directorate General of Hydrocarbons, New Delhi.
Collett, T.S., Agena, W.F., Lee, M.W., Zyrianova, M.V., Bird, K.J., Charpentier, R.R., Cook, T., Houseknecht, D.W., Klett, T.R., Pollastro, R.M., Schenk, C.J., 2008b. Assessment of Gas Hydrates Resources on the North Slope, Alaska. U.S. Geological Survey, fact Sheet 2008–3073, 4 p.
Cook, A.E, Goldberg, D., 2008a. Stress and Gas Hydrate-filled Fracture Distribution, Krishna–Godavari Basin, India. Proceedings of the 6th International Conference on Gas Hydrates, 6–10 July, Vancouver, BC, Canada.
Cook, A.E., Goldberg, D., 2008b. Extent of gas hydrate filled fracture planes: implication for in situ methanogenesis and resource potential. Geophys. Res. Lett. 35, L15302. doi:10.1029/2008GL034587.
Dai, J., Fred, S., Diana, G., Adam, K., Dutta, N., 2008. Exploration for gas hydrates in the deepwater, northern Gulf of Mexico: Part I, A seismic approach based on geologic model, inversion, and rock physics principles. Mar. Petr. Geol. 25, 830–844.
Dvorkin, J., Nur, A., 1993. Rock Physics for Characterization of Gas Hydrates, The Future of Energy Gases. U.S. Geological Survey. Professional Paper, 1570.
Dvorkin, J., Prasad, M., Sakai, A., Lavoie, D., 1999. Elasticity of marine sediments: rock physics modeling. Geophy. Res. Lett. 26, 1781–1784.
Fofonoff, N.P., 1985. Physical properties of seawater: a new salinity scale and equation of state for seawater. J. Geophys. Res. 90 (C2), 3332–3342. doi:10.1029/JC090iC02p03332.
Frye, M., Grace, J., Hunt, J., Kaufman, G., Schuenemeyer, J., Shedd, B., 2008. MMS Releases preliminary results of Gulf of Mexico In-Place natural gas hydrate assessment. http://www.netl.de.gv/technologies/oilgas/publications/Hydrates/Newsletter/HMNewsSpring08.pdf National Energy Technology Laboratory (NETL) Fire in the Ice Methane Hydrate Newsletter.

Guerin, G., Goldberg, D., Melsterl, A., 1999. Characterization of in situ elastic properties of gas hydrate-bearing sediments on the Blake Ridge. J. Geophy. Res. 104, 17781–17796.

Hearst, J.R., Nelson, P.H., Paillett, F.L., 2000. Well Logging for Physical Properties-a Handbook for Geophysicists, Geologists and Engineers. John Wiley and Sons, New York, pp. 484.

Helgerud, M.B., Dvorkin, J., Nur, A., 1999. Elastic-wave velocity in marine sediments with gas hydrates: effective medium modeling. Geophy. Res. Lett. 26, 2021–2024.

Hilfer, R., 1991. Geometric and dielectric characterization of porous media. Phys. Rev. 44 (1), 60–75. doi:10.1103/PhysRevB.44.60.

Hyndman, R.D., Moore, G.F., Moran, K., 1993. Velocity, porosity, and pore-fluid loss from the Nankai subduction zone accretionary prism. Proc. Ocean. Drill. Prog. Sci. Results 131, 211–220.

Hyndman, R.D., Spence, G.D., Chapman, N.R., Riedel, M., Edwards, R.N., 2001. Geophysical studies of marine gas hydrate in northern Cascadia. In: Paull, C.K., Dillon, W.P. (Eds.), Natural Gas Hydrates: Occurrence, Distribution, Detection. American Geophysical Union Monographs, vol. 124, pp. 273–295.

Hyndman, R.D., Yuan, T., Moran, K., 1999. The concentration of deep sea gas hydrates from downhole electrical resistivity logs and laboratory data. Earth Planet. Sci. Lett. 172 (1–2), 167–177. doi:10.1016/S0012-821X(99)00192-2.

Ioannidis, M.A., Kwiecien, M.J., Chatzis, I., 1997. Electrical conductivity and percolation aspects of statistically homogeneous porous media. Transp. Porous Media 29 (1), 61–83. doi:10.1023/A:1006557614527.

Jackson, P.D., Taylor, S.D., Stanford, P.N., 1978. Resistivity-porosity-particle shape relationships for marine sands. Geophysics 43 (6), 1250–1268. doi:10.1190/1.1440891.

Kleinberg, R.L., Flaum, C., Straley, C., Brewer, P.G., Malby, G.E., Peltzer, E.T., Friederich, G., Yesinowski, J.P., 2003. Seafloor nuclear magnetic resonance assay of methane hydrate in sediment and rock. J. Geophys. Res. 108, 2137. doi:10.1029/2001JB000919.

Kleinberg, R.L., Flaum, C., Collett, T.S., 2005. Magnetic resonance log of JAPEX/JNOC/GSC et al. Mallik 5L-38 gas hydrate production research well: gas hydrate saturation, growth habit, relative permeability. In: Dallimore, S.R., Collett, T.S. (Eds.), Scientific Results from the Mallik 2000 Gas Hydrate Production Research Well Program. Geological Survey of Canada Bulletin, vol. 585, p. 10. Mackenzie Delta, Northwest Territories, Canada.

Kvenvolden, K.A., Ginsburgh, G.D., Soloviev, V.A., 1993. Worldwide distribution of subaquatic gas hydrates. Geo-Mar. Lett. 13, 32–40.

Lee, M.W., Hutchinson, D.R., Dillon, W.P., Miller, J.J., Agena, W.F., Swift, B.A., 1993. Method of estimating the amount of in situ gas hydrates in deep marine sediments. Mar. Petro. Geol. 10, 496–506.

Lee, M.W., Collett, T.S., 2005. Assessments of gas hydrate concentrations estimated from sonic logs in the Mallik 5L-38 well, N.W.T., Canada. In: Dallimore, S.R., Collett, T.S. (Eds.), Scientific Results for Mallik 2002 Gas Hydrate Production Research Well Program. Geological Survey of Canada Bulletin, vol. 585, p. 10. Mackenzie Delta, Northwest Territories, Canada.

Lee, M.W., Collett, T.S., 2008. Integrated analysis of well logs and seismic data at the Keathley Canyon, Gulf of Mexico, for estimation of gas hydrate concentrations. Mar. Petro. Geol. 25, 924–931.

Lee, M.W., Waite, W.F., 2008. Estimating pore-space gas hydrate saturations from well-log acoustic data. Geochem. Geophys. Geosyst. 9 (8), Q07008. 10, 1029/2008GC002081.

Lee, M.W., Collett, T.S., 2009. Gas hydrate saturations estimated from fractured reservoir at Site NGHP-01-10, Krishna-Godavari Basin, India. J. Geophy. Res. 114, B07102. doi:10.1029/2008JB006237.

Mathews, M., 1986. Logging characteristics of methane hydrate. Log Anal. 27, 26–63.

Mazumdar, A., Dewangan, P., Joao, H.M., Peketi, A., Khosla, V.R., Kocherla, M., Badesab, F.K., Joshi, R.K., Roxanne, P., Ramamurty, P.B., Karisiddaiah, S.M., Patil, D.J., Dayal, A.M., Ramprasad, T., Hawkesworth, C.J., Avanzinelli, R., 2009. Evidence of paleo–cold seep activity from the Bay of Bengal, offshore India. Geochem. Geophys. Geosyst 10 (6), 15. doi:10.1029/2008GC002337.

Paull, C.K., Matsumoto, R., Wallace, P.J., et al., 1996. Proceedings of the Ocean Drilling Program, Init. Rep, vol. 164. Ocean Drilling Program, College Station, TX, 623 pp.

Pearson, C.F., Halleck, P.M., McGuire, P.L., Hermes, R., Mathews, M., 1983. Natural gas hydrate: a review of in situ properties. J. Phys. Chem. 87, 4180–4185.

Ramana, M.V., Ramprasad, T., Paropkari, A.L., Borole, D.V., Rao, B.R., Karisiddaiah, S.M., Desa, M., Kocherla, M., Joao, H.M., Lokabharati, P., Gonsalves, M.J., Pattan, J.N., Khadge, N.H., Babu, C.P., Sathe, A.V., Kumar, P., Sethi, A.K., 2009. Multidisciplinary investigations exploring indicators of gas hydrate occurrence in the Krishna–Godavari Basin offshore, east coast of India. Geo-Mar. Lett. 29, 25–38.

Riedel, M., Bellefleur, G., Mair, S., Brent, T.A., Dallimore, S.R., 2009. Acoustic impedance inversion and seismic reflection continuity analysis for delineating gas hydrate resources near the Mallik research sites, Mackenzie Delta, Northwest Territories, Canada. Geophysics 74 (5), B125–B137.

Schlumberger, 1989. Log Interpretation Principles/Applications. TX (Schlumberger Educational Services), Houston.

Shankar, U., Riedel, M., Sathe, A.V., 2010. Geothermal modeling of the gas hydrate stability zone along the Krishna–Godavari basin. Mar. Geophy. Res., in press, doi:10.1007/s11001-010-9089-6.

Spangenberg, E., 2001. Modeling of the influence of gas hydrate content on the electrical properties of porous sediments. J. Geophys. Res. 106 (B4), 6535–6548. doi:10.1029/2000JB900434.

Stoll, R.D., Ewing, J.I., Bryang, M., 1971. Anomalous wave velocities in sediments containing gas hydrates. J. Geophys. Res. 76, 2090–2094.

Swanson, B.F., 1979. Visualizing pores and non-wetting phase in porous rock. J. Pet. Technol. 31 (1), 10–18. doi:10.2118/6857-PA.

Tucholkeb, E., Bryang, M., Ewing, J.I., 1977. Gas hydrate horizons detected in seismic-profiler data from the western North Atlantic. Amer. Assoc. Pet. Geol. Bull. 61, 698–707.

Westbrook, G.K., Carson, B., Musgrave, R.J., et al., 1994. Proceedings of the Ocean Drilling Program, Init. Rep, 146. Ocean Drilling Program, College Station, TX.

Yuan, T., Hyndman, R.D., Spence, G.D., Desmons, B., 1996. Seismic velocity increase and deep-sea gas hydrate concentrations above a bottom-simulating reflector on the northern Cascadia continental slope. J. Geophys. Res. 101, 13655–13671.